Laser Flash Photolysis Studies of Radical−Radical Reaction Kinetics: The HO_2 + BrO Reaction

J. M. Cronkhite,[†] R. E. Stickel,[‡] J. M. Nicovich,[‡] and P. H. Wine*[,‡,§]

Georgia Institute of Technology, Atlanta, Georgia 30332

Received: March 11, 1998; In Final Form: June 3, 1998

Laser flash photolysis of $Cl_2/CH_3OH/O_2/Br_2/O_3/N_2$ mixtures at 308 nm has been coupled with simultaneous time-resolved detection of HO_2 (by infrared tunable diode laser absorption spectroscopy) and BrO (by ultraviolet absorption spectroscopy) to investigate the kinetics of the important stratospheric reaction HO_2 + BrO → products at 296 ± 3 K in N_2 buffer gas at pressures of 12 and 25 Torr. All experiments were performed under near pseudo-first-order conditions with HO_2 in excess over BrO. The HO_2 + BrO rate coefficient is found to be $k_1 = (2.0 \pm 0.6) \times 10^{-11}$ cm^3 molecule^{-1} s^{-1}, with the primary source of uncertainty being knowledge of the infrared line strength(s) required to convert measured HO_2 absorbances to absolute concentrations. The rate coefficient for the reaction $HO_2 + HO_2 \rightarrow H_2O_2 + O_2$ derived based on infrared absorption measurements of the HO_2 concentration is consistent with the currently accepted value. The results reported in this study are compared with other recent studies of HO_2 + BrO kinetics, and their implications for our understanding of stratospheric chemistry are discussed.

Introduction

It has been recognized for two decades that bromine in the stratosphere can act as an ozone removal catalyst analogous to chlorine.[1] The gas-phase catalytic cycle,

$$HO_2 + BrO \rightarrow HOBr + O_2 \quad (1)$$

$$HOBr + h\nu \rightarrow Br + OH \quad (2)$$

$$Br + O_3 \rightarrow BrO + O_2 \quad (3)$$

$$OH + O_3 \rightarrow HO_2 + O_2 \quad (4)$$

Net: $2O_3 \rightarrow 3O_2$

for which reaction 1 is the rate-limiting step, was first suggested in 1980.[2] Estimates of the rate coefficient for reaction 1 (k_1) at that time rendered the above cycle too slow to contribute significantly to odd oxygen loss compared to the Br/Cl cycle:

$$Br + O_3 \rightarrow BrO + O_2 \quad (3)$$

$$Cl + O_3 \rightarrow ClO + O_2 \quad (5)$$

$$ClO + BrO \rightarrow Br + Cl + O_2 \quad (6)$$

Net: $2O_3 \rightarrow 3O_2$

The first attempt to directly measure k_1 was reported by Cox and Sheppard[3] in 1982 and employed the molecular modulation technique with UV absorption detection; their reported room-temperature rate coefficient of 5.0×10^{-12} cm^3 molecule^{-1} s^{-1} seemed to confirm that the HO_2 + BrO cycle was, indeed, of little importance in stratospheric chemistry. This remained the recommended rate coefficient for use in atmospheric modeling for the following 10 years. A report appeared in 1992 of the results of a discharge flow experiment performed by Poulet et al. that indicated that k_1 at 298 K is in fact more than 6 times faster than the Cox and Sheppard result suggested.[4] Poulet and co-workers also performed simulation-based analyses, which showed that, at their reported value of k_1, the catalytic cycle defined by reactions 1−4 is significant in determining the overall partitioning of bromine in the stratosphere, as well as bromine-mediated ozone loss; this applies in particular in the lower stratosphere, where the BrO + ClO cycle, i.e., reactions 3, 5, and 6, also has a major impact. The importance of k_1 for understanding ozone chemistry of the lower midlatitude stratosphere was further underscored by the results of the Stratospheric Photochemistry, Aerosols, and Dynamics Expedition (SPADE), which provided simultaneous in situ measurements of several important radical species.[5] Since 1992 a number of studies of reaction 1 have been published,[6−9] including three temperature-dependent studies.[6,8,9] While there exists excellent agreement between reported activation energies for reaction 1 ($E_a \sim -4.5$ kJ mol^{-1}), recently reported values for k_1(298 K) span the undesirably wide range $(1.4-3.4) \times 10^{-11}$ cm^3 molecule^{-1} s^{-1}.

In this paper, we report a study of the room-temperature (296 ± 3 K) kinetics of the HO_2 + BrO reaction. This work builds on our previously reported studies of the kinetics of reactions of $O(^3P_J)$ with HO_2,[10,11] ClO,[12] and BrO.[13] As is the case with a majority of radical−radical reactions of atmospheric interest, most recent studies of HO_2 + BrO kinetics have employed discharge flow (rather than flash photolysis) methods. Comparison of kinetic data obtained using very different experimental methods is one useful means for elucidating systematic errors in the different experimental approaches. Results reported in this paper are discussed in light of our current understanding of stratospheric bromine chemistry and in light of the discrepancies in the existing literature values for k_1(298 K).

[†] School of Physics.
[‡] Georgia Tech Research Institute.
[§] School of Chemistry and Biochemistry and School of Earth and Atmospheric Sciences.

S1089-5639(98)01456-X CCC: $15.00
Published on Web 07/24/1998

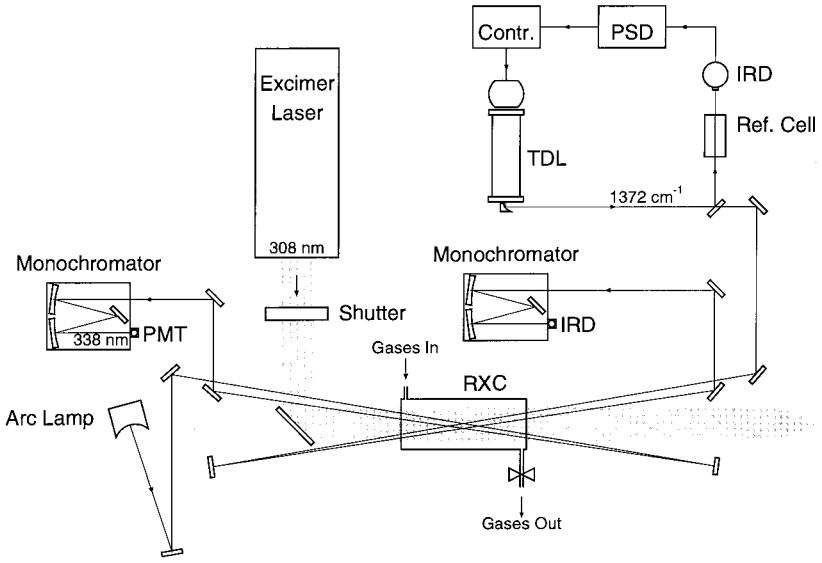

Figure 1. Schematic diagram of the experimental apparatus. Contr. = controller; IRD = infrared detector; PMT = photomultiplier tube; PSD = phase-sensitive detector; Ref. = reference; RXC = reaction cell.

Experimental Technique

This study employed 308 nm pulsed laser (20 ns pulse width, ~50 mJ cm^{-2} $pulse^{-1}$) photolysis of $N_2/O_2/CH_3OH/Cl_2/O_3/Br_2$ mixtures in conjunction with simultaneous time-resolved detection of HO_2 (by infrared tunable diode laser absorption spectroscopy at 1372 cm^{-1}) and BrO (by UV absorption spectroscopy at 338.3 nm) to study HO_2 + BrO reaction kinetics at 296 ± 3 K and pressures of 25 and 12 Torr. HO_2 radicals were generated via the reaction scheme

$$Cl_2 + h\nu\ (308\ nm) \rightarrow 2Cl(^2P_J) \qquad (7)$$

$$Cl(^2P_J) + CH_3OH \rightarrow CH_2OH + HCl \qquad (8)$$

$$CH_2OH + O_2 \rightarrow HO_2 + CH_2O \qquad (9)$$

which produced maximum HO_2 concentrations of (7−24) × 10^{13} molecules cm^{-3} under the conditions employed. BrO radicals at maximum concentrations in the range (7−13) × 10^{12} molecules cm^{-3} were simultaneously generated as follows:

$$O_3 + h\nu\ (308\ nm) \rightarrow O(^1D_2) + O_2(a\ ^1\Delta_g) \qquad \Phi = 0.80^{14} \qquad (10)$$

$$\rightarrow O(^3P_J) + O_2(X\ ^3\Sigma_g^-) \qquad \Phi = 0.20$$

$$O(^1D_2) + M \rightarrow O(^3P_J) + M, \quad M = N_2, O_2 \qquad (11)$$

$$Br_2 + O(^3P_J) \rightarrow BrO + Br(^2P_J) \qquad (12)$$

$$Br(^2P_J) + O_3 \rightarrow BrO + O_2 \qquad (13)$$

Because HO_2 is the excess reagent under the conditions employed, the accuracy of the derived rate coefficient depends critically on accurate measurement of the HO_2 concentration, but is only weakly dependent on knowledge of the absolute concentration of BrO. However, it is the BrO temporal profile that is a sensitive indicator of the BrO + HO_2 rate coefficient.

All experiments were carried out at room temperature (296 ± 3 K) at either 25 or 12 Torr total pressure under "slow flow" conditions (flow rate ~5 cm s^{-1} through the photolysis region); at a laser flash repetition rate of 0.25 Hz, this allowed for replenishment of the reagents between laser flashes, thus preventing accumulation of reaction and photolysis products in the reactor. O_3 concentrations were measured in the flow system upstream from the reaction cell using UV photometry at 253.7 nm (Hg penray lamp light source). A correction due to a slight pressure drop between the UV photometry cell and the reaction cell was made to determine the O_3 concentration in the reaction cell itself; the correction was always ≤5%. Concentrations of all other gases in the mixture were determined from their measured relative mass flow rates into the system, source concentrations (some compounds used were diluted in 12 L Pyrex bulbs; see below), and the total system pressure. Laser pulse energy was monitored continuously using the internal energy meter of the laser (Lambda Physik Lextra 200); an absolute calibration was obtained using a thermopile calorimeter energy meter (Scientech model 38-0105) at least once per day. The energy thus measured was corrected for window losses (measured to be < 10%) and reflections within the cell to derive an estimate of the laser pulse energy in the reaction zone. Shot-to-shot laser pulse energy variations were less than 2% on average, and the cross-sectional spatial intensity variations in the photolysis beam were measured to be less than 10% for the portion of the beam that irradiated the detection volume. Because (1) the cell length along the photolysis axis was only 15 cm and (2) the beam traveled several meters before entering the cell, beam divergence through the photolysis region was expected to be minimal; this was confirmed by measurements of laser fluence as a function of position with the cell removed from the beam path.

A schematic diagram of the apparatus is shown in Figure 1. The concentration of BrO was monitored using UV absorption at 338.3 nm, the peak of the strong 7−0 band of the $A^2\pi-X^2\pi$ system. A 150 W high-pressure xenon arc lamp was used as a light source for the BrO absorption measurements. The arc lamp beam was passed twice through the reaction region nearly collinearly to the 308 nm pulsed photolysis laser, giving an effective absorption path length of 30.8 cm. Masks of 1.0 cm × 3.5 cm on the front and rear of the cell confined the arc lamp beam to the laser photolysis region. A 0.22 m monochromator tuned to 338.3 nm (resolution 0.38 nm) was used to isolate the desired wavelength and a UV-sensitive photomultiplier tube monitored the light level. The time-dependent

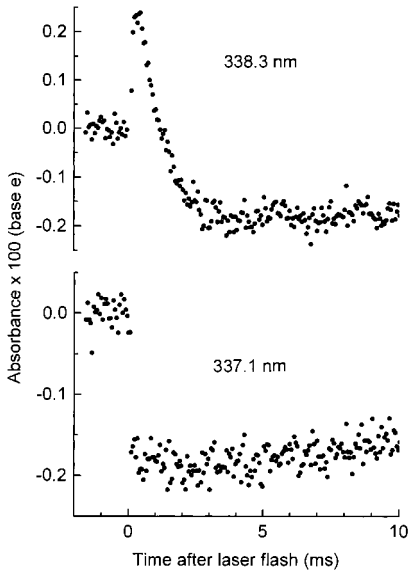

Figure 2. Observed absorbance temporal profiles at 338.3 and 337.1 nm under the conditions of expt no. 13 (see Table 2).

current output of the photomultiplier was sent through a fixed resistor (50 μs *RC* time constant), and the resulting voltage was monitored by a signal averager with 10 bit voltage resolution. Data acquisition was pretriggered relative to the laser flash to obtain I_0, the 338.3 nm light level prior to BrO production. The 298 K BrO absorption cross section at 338.3 nm reported by Wahner et al.,[15] 1.55×10^{-17} cm^2, was used to convert measured BrO absorbances to absolute concentrations using the Beer−Lambert law,

$$[\mathrm{BrO}] = \frac{\ln(I_0/I_t)}{\sigma_{\mathrm{BrO}} l} \qquad \text{(I)}$$

where I_t is the 338.3 nm light level at a time t after the laser flash, σ_{BrO} is the BrO absorption cross section, and l is the path length.

BrO detection was complicated by the fact that Cl_2 absorbs at the BrO monitoring wavelength, 338.3 nm. When the 308 nm laser fires, the concentration of Cl_2 in the reaction mixture is reduced slightly by photolysis, thereby increasing the level of 338.3 nm light transmitted. This increase appears as a sudden jump in the absorption-derived BrO level at the time of the laser pulse (see Figure 2). Furthermore, the level of absorbance due to Cl_2 does not remain perfectly constant after the laser flash, but slowly recovers back to the preflash baseline due to diffusion and gas flow through the cell. To correct for these effects, an empirical approach was employed that utilized the fact that the BrO absorption spectrum is highly structured near 338 nm, whereas the Cl_2 absorption cross section changes very slowly as a function of wavelength in the 338 nm region. Identical experiments were performed back to back in which the 0.22 m monochromator was alternately tuned to 338.3 and 337.1 nm, the latter wavelength being a valley in the BrO spectrum where absorbance is reduced to 5−10% of the peak value (Cl_2 absorbance changes by less than 1% over the same region). Figure 2 shows a sample absorbance temporal profile at 337.1 nm. Since the magnitude of the baseline transmittance jump is dependent upon the Cl_2 concentration (given constant laser power), the entire range of employed Cl_2 concentrations was investigated in this manner. Figure 3 shows a plot of the absorbance jump at 337.1 nm as a function of $[Cl_2]$. The

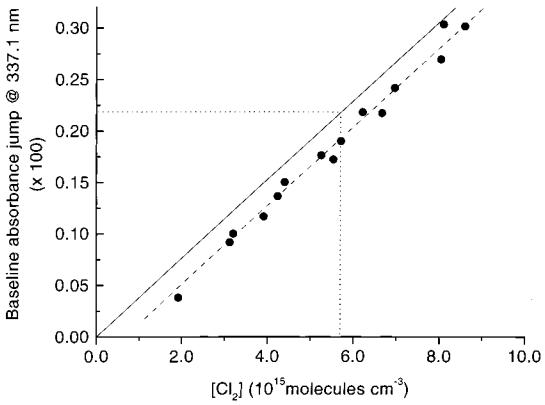

Figure 3. Plot of Cl_2 concentration vs baseline correction needed to bring the 337.1 nm postflash baseline into line with the preflash baseline. The points represent the observed displacement from the preflash baseline absorbance at 337.1 nm. The dashed line is a linear regression fit to the points. Vertical and horizontal dotted lines indicate $[Cl_2]$ and the baseline correction applied to the 338.3 nm absorbance profile, respectively, for expt no. 13 (see Table 2).

relationship is linear as expected, but does not intersect the origin (i.e., zero jump at zero $[Cl_2]$) as might be expected. The reason for this is that there is some absorption from BrO contributing to the measured jump; the BrO absorbance at 337.1 nm is not quite zero. However, although the intercept of the line in Figure 3 is affected by this slight BrO absorption, its slope is not. Therefore the "true" value of the baseline jump (i.e., the amount due solely to Cl_2) at a given $[Cl_2]$ can be derived simply by shifting the entire line so that it intersects the origin without any change in the slope. The resulting correction can be applied to the absorbance temporal profiles measured at 338.3 nm. To correct for the drift in Cl_2 transmittance back toward the preflash baseline, an analytical curve (exponential decay of the form $\alpha e^{-\beta t} - \delta$) was fit to the 337.1 nm absorbance temporal profiles at times after 2 ms and then subtracted from the 338.3 nm BrO absorbance temporal profile. A corrected BrO concentration temporal profile is shown in Figure 5.

HO_2 radicals were detected via time-resolved IR tunable diode laser (TDL) absorption at 1371.927 cm^{-1}. The output from an IR TDL was passed twice through the (masked) photolysis region of the reaction cell collinearly with the 308 nm laser beam, giving an absorption path length of 30.8 cm. The IR beam was then passed through a 0.5 m monochromator (to isolate the desired TDL mode) to a HgCdTe detector cooled to 77 K. The detector output was monitored by a signal averager for digitization, storage, and further analysis. Baseline data were obtained between laser shots, averaged, and subtracted from the HO_2 signal measurements. Isolation by the monochromator of a single mode of the TDL output was confirmed by verifying 100% absorption by a high concentration of SO_2 at 1371.934 and 1371.885 cm^{-1}.

The TDL was modulated at 2 kHz over a narrow spectral region surrounding 1371.927 cm^{-1}. A portion of the output beam was picked off and passed through a reference cell containing CH_3Cl, which has an IR absorption line nearly coincident with the HO_2 line being used, and then to a second IR detector. The output from this detector was used to generate a phase-dependent feedback signal to keep the modulation region centered around the CH_3Cl (and hence, HO_2) absorption line.

Absolute HO_2 concentrations were determined from the integrated line strength at 1371.927 cm^{-1} reported by Zahniser et al.[16] A plot of a typical TDL data set from which absolute $[HO_2]$ was determined is shown in Figure 4. Integrated absorption was determined by numerical integration of the area

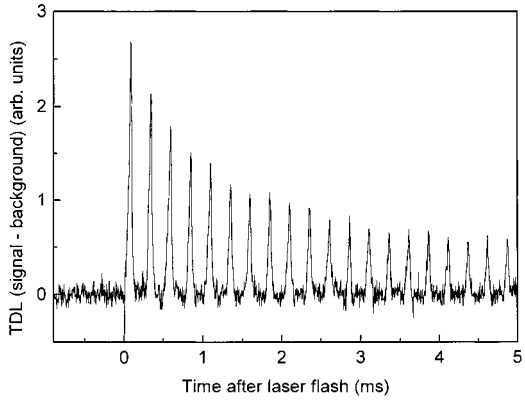

Figure 4. Plot of TDL signal minus baseline for expt no. 13 (see Table 2). Absolute HO_2 concentration temporal profiles were derived from the observed peak heights as described in the text.

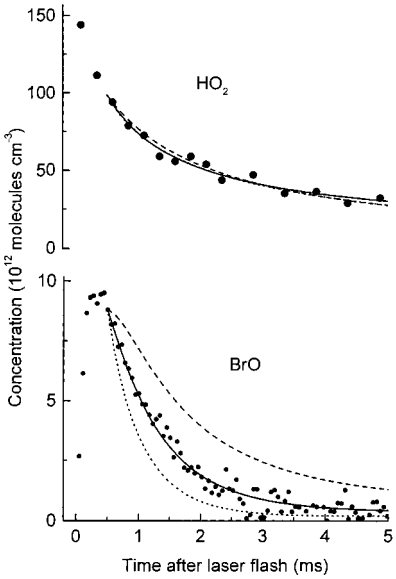

Figure 5. Simulated temporal profiles generated from numerical integration of the rate equations using the chemical model given in Table 1. As in Figure 2, the data are from expt no. 13 (see Table 2). Points are measured data. Solid line: $k_1 = 2.04 \times 10^{-11}$ cm^3 molecule^{-1} s^{-1} (the best fit value). Dotted line: simulation with $k_1 = 1.0 \times 10^{-11}$ cm^3 molecule^{-1} s^{-1}; dashed line: simulation with $k_1 = 3.0 \times 10^{-11}$ cm^3 molecule^{-1} s^{-1}.

under the HO_2 peaks in the digitized signal, using

$$S = \frac{1}{nl}\int \ln\frac{I_0}{I(\nu)}\,d\nu = \frac{1}{nl}\int \ln\frac{I_0}{I_0 - y(\nu)}d\nu \qquad \text{(II)}$$

where S is the integrated line strength, n is the HO_2 number density, l is the absorption path length, I_0 and $I(\nu)$ are the absolute detected IR signal levels before and after HO_2 production, respectively, and $y(\nu)$ is the detected signal deviation from the zero-absorbance baseline. The results were then calibrated to peak absorption at a given pressure, so that peak absorbance could be used as a proxy for total absorbance. The absolute baseline IR intensity at the detector, I_0, was determined either by mechanically chopping the beam at 1 kHz or by inference from the measured integrated absorbance of a known concentration of SO_2 at 1371.934 cm^{-1} ([SO_2] was measured in situ using UV photometry at 253.7 nm); the two methods agreed to within 5%. A typical measured HO_2 concentration profile is shown in Figure 5.

Two secondary checks of the absolute HO_2 concentration were also available in this experiment. One was to observe the temporal profile of HO_2 in the absence of Br_2/O_3 to determine the HO_2 loss rate. Under these conditions HO_2 loss is determined solely (aside from very slow background losses) by the reaction

$$HO_2 + HO_2 \rightarrow H_2O_2 + O_2 \qquad (14)$$

The HO_2 concentration is then related to the rate constant k_{14} via

$$\frac{1}{[HO_2]_t} = \frac{1}{[HO_2]_0} + 2k_{14}t \qquad \text{(III)}$$

where $[HO_2]_t$ is the HO_2 concentration at a time t after the laser flash and $[HO_2]_0$ is the peak HO_2 concentration. The [HO_2] absorbance data were calibrated so that a linear least-squares fit of the $[HO_2]_t^{-1}$ versus t data gave the literature value of $2k_{13}$ (2.4×10^{-12} cm^3 molecule^{-1} s^{-1} at 296 K[14]) as the slope at each of the two pressures employed (the pressure-dependent component of k_{14} accounts for only 1−2% of the total rate constant in the 12−25 Torr pressure range). This procedure results in HO_2 concentrations that are a factor of 1.05 ± 0.10 (error is 2σ, precision only) times larger than concentrations deduced from the 1372 cm^{-1} absorption line strength calibrations.

Another check on absolute [HO_2] was Cl atom titration. HO_2 production in the absence of Br_2/O_3 is nearly identical to [Cl] produced from Cl_2 photolysis; that is, the chlorine atoms are completely titrated to HO_2 via reactions 8 and 9. $[Cl]_0$, the chlorine atom concentration initially produced by the laser flash, was determined from

$$[Cl]_0 = 2[Cl_2]E\frac{\sigma\lambda}{hc} \qquad \text{(IV)}$$

where [Cl_2] is the molecular chlorine concentration prior to the laser flash, E is the laser pulse energy per unit area, σ is the 308 nm absorption cross section for Cl_2, λ is the laser wavelength, h is Planck's constant, and c is the speed of light. This [HO_2] determination method gave results in excellent agreement with the two aforementioned methods within the estimated uncertainty, which is primarily due to spatial variations in the photolysis beam, uncertainty in the Cl_2 concentration, and uncertainty in the minor contribution of the $Cl + O_3$ reaction to Cl removal. Both secondary checks on HO_2 concentrations were carried out for each value of [HO_2] investigated.

The compounds used in this study had the following stated minimum purities: N_2 99.999%, O_2 99.99%, Cl_2 99.99%, SO_2 99.98%, Br_2 99.94%, CH_3OH 99.9%; in the cases of Cl_2 and SO_2, the stated purity refers to the liquid phase in the high-pressure gas cylinder. Molecular chlorine, CH_3OH, Br_2, and SO_2 were degassed repeatedly at 77 K and then diluted in N_2; the resulting mixtures were stored in 12 L Pyrex bulbs. Ozone was prepared by passing O_2 (99.99% stated purity) through a commercial ozonator. It was collected and stored on refrigeration grade silica gel at a temperature of 195 K.

Data Analysis

A chemical model of the experimental reaction system was developed to analyze the results. To most efficiently describe the system chemistry, the model was divided into two temporal regions: $t \leq 500$ μs and $t > 500$ μs. Initially, the laser flash produces a large number of radical species, and the resulting chemistry is very complex. However, most of the radicals are converted to HO_2 or BrO within 500 μs of the laser flash, greatly

TABLE 1: Chemical Model for Simulating Observed BrO + HO_2 Temporal Profiles. Bimolecular Rate Coefficients Are from Ref 14, Unless Otherwise Indicated

reactants	products	k (cm^3 $molecule^{-1}$ s^{-1})
$BrO + HO_2$	$HOBr + O_2$	variable
$BrO + BrO$	$Br_2 + O_2$	4.4×10^{-13}
$BrO + BrO$	$Br + Br + O_2$	2.3×10^{-12}
$BrO + ClO$	$Br + OClO$	1.4×10^{-11}
$BrO + ClO$	$BrCl + O_2$	1.0×10^{-12}
$Br + O_3$	$BrO + O_2$	1.2×10^{-12}
$Br + H_2CO$	$HBr + HCO$	1.1×10^{-12}
$HO_2 + HO_2$	$H_2O_2 + O_2$	1.7×10^{-12}
$HO_2 + ClO$	$HOCl + O_2$	5.0×10^{-12}
$O_2(a\ ^1\Delta_g) + O_3$	$O + O_2 + O_2$	3.8×10^{-15}
$O + Br_2$	$BrO + Br$	2.0×10^{-11} [a]
$O + HO_2$	$OH + O_2$	5.9×10^{-11}
$O + ClO$	$Cl + O_2$	3.8×10^{-11}
BrO	background loss	25 s^{-1} [b]
HO_2	background loss	25 s^{-1} [b]
$O_2(a\ ^1\Delta_g)$	background loss	25 s^{-1} [b]

[a] From ref 24. [b] Estimates.

simplifying the system chemistry. It was found that a simplified chemical model could be used for the analysis after $t = 500$ μs without loss of integrity, as shown by direct comparison with the results of the more complex model starting from $t = 0$; this simplified chemical model is given in Table 1.

All rate coefficients in Table 1 are taken from the literature except the background loss rates for HO_2, BrO, and $O_2(^1\Delta_g)$, which represent the effects of net diffusion of radicals out of the detection region and reactions with minor impurities in the gas mixture. The background loss rate for BrO was estimated by observing BrO loss in the absence of HO_2 for various BrO concentrations, with special weight given to lower concentrations (which minimize the contribution from the BrO + BrO reaction). An extra exponential decay term was required to achieve good fits between the simulated BrO profiles and the observed profiles under these conditions; the average rate of this decay term was taken as the background loss rate. Because detection was not as sensitive for HO_2 as for BrO, HO_2 loss could not be studied at low enough concentrations (and hence, slow enough HO_2 self-reaction loss rates) for the above procedure to give definitive results. Therefore the HO_2 background loss rate and that for $O_2(^1\Delta_g)$ were assumed to be the same as that found for BrO. The overall error in k_1 introduced by uncertainties in the background radical loss rates is very small because (1) k_1 is sensitive to the absolute instantaneous value of $[HO_2]$ (which was measured directly), but not its time derivative, and (2) the BrO background loss rate is much smaller than the loss rates due to reaction 1, which are in the range 1200−4800 s^{-1}.

Simulations demonstrate that once BrO and HO_2 production are complete, HO_2 loss is due primarily to its self-reaction and BrO loss is overwhelmingly dominated by reaction with HO_2. Under these conditions the rate coefficient for reaction 1, k_1, and the HO_2 concentration temporal profile are the strongest determinants of the shape of the BrO temporal profile. To find the experimental value for k_1, the differential equations describing the time rates of change of the chemical species in the simplified model (Table 1) were integrated numerically under exact experimental conditions while iteratively varying k_1 to achieve a best fit to the measured HO_2 and BrO concentration temporal profiles; in this fitting procedure, k_1 was the *only* adjustable parameter.

Due to differences in the HO_2 and BrO measurement and data collection techniques, data collection could not be synchronized between the two. For the inputs to the numerical integration routine, however, synchronous HO_2 and BrO data were required. Therefore, HO_2 concentrations at times intermediate to the measured values were inferred by interpolation along a smooth analytical function fit to the HO_2 data via nonlinear least-squares analysis. The function used was of the form $(\alpha + 2\beta t)^{-1}$, which is the theoretical form of the decay profile assuming the HO_2 + HO_2 reaction dominates. This approach was compared with several other interpolation methods (data smoothing, polynomial spline) and was judged superior.

The analyses for deriving k_1 were performed using a commercial software package designed for the purpose (FACSIMILE release 3.05, United Kingdom Atomic Energy Authority). Figure 5 shows the simulated decay profiles of HO_2 and BrO, respectively, resulting from the analysis of a typical experiment, along with the measured profiles for comparison. To demonstrate the sensitivity of the data to k_1, simulated temporal profiles that employed k_1 values somewhat higher and somewhat lower than the best fit value are also shown; as discussed above, the BrO temporal profile provides a sensitive indicator of k_1, whereas the HO_2 temporal profile is relatively insensitive to k_1.

To determine the sensitivity of the results to variations in the input parameters, several analyses were performed in which the reactant concentrations and assumed rate coefficients were independently and systematically varied. The final value of k_1 was found to vary in approximately inverse proportion to the peak HO_2 concentration, as would be expected under truly pseudo-first-order conditions. Variations in [BrO] which reflected a ±15% uncertainty in the 338.3 nm absorption cross section,[15] on the other hand, produced a change of less than 3% in the resulting mean k_1 derived from the analysis and no discernible trend for positive versus negative changes in the absorption cross section. The rate coefficient for the ClO + BrO reaction was also varied within the limits of its estimated uncertainty (±25%)[14] to determine its potential contribution to the uncertainty in the value of k_1. ClO is formed via Cl + O_3, a minor competitor to reaction 6, during the first few microseconds after the laser pulse, and could account for up to 5% of the BrO loss rate at peak ClO concentrations; it was found to be an insignificant contributor to the uncertainty in k_1. Finally, variations by factors of 5 (up or down) in the initial estimated value of k_1 input to the model had no effect on the value of k_1 to which the simulations ultimately converged.

Although the mechanism in Table 1 contains 16 reactions, observed BrO and HO_2 kinetics were dominated by the HO_2 + BrO and HO_2 + HO_2 reactions. In fact, values for k_1 obtained by fitting observed BrO temporal profiles to a mechanism containing *only* these two reactions were found to differ from those obtained using the full mechanism by only a few percent. When the two-reaction scheme was employed, however, systematic deviations between observed and simulated BrO temporal profiles were observed at long times which are attributable to BrO regeneration via the reaction sequence 15, 12, and 13

$$O_2(^1\Delta_g) + O_3 \rightarrow O(^3P_J) + 2O_2 \qquad (15)$$

In addition to the chemical schemes used to generate HO_2 and BrO, i.e., reactions 7−13, numerous other radical reactions occurring on short time scales warrant consideration as potential interferences to clean measurement of the HO_2 + BrO rate coefficient. A key issue is whether any radical species other than HO_2 generated during the first 500 μs after the laser flash reach sufficient levels to significantly affect the BrO temporal profile at $t > 500$ μs. To address this question, detailed simulations of the chemistry at $t < 500$ μs were carried out for the exact conditions employed to obtain each BrO temporal

TABLE 2: Summary of Experimental Results

		concentration[a] (10^{13} cm^{-3})						10^{11} k_1(298 K)
expt no.	P (Torr)	Cl_2	O_3	Br_2	CH_3OH	$HO_{2\ max}$	BrO_{max}	(cm^3 molecule^{-1} s^{-1})
1	25	568	245	12.2	987	12.3	0.98	1.90
2	25	762	233	15.6	1020	16.1	0.80	1.90
3	25	603	238	14.5	1000	13.1	1.01	2.07
4	25	447	231	17.3	1010	11.3	1.09	1.89
5	25	643	239	14.3	1160	14.5	0.90	1.89
6	25	346	234	19.2	1150	8.6	1.27	1.84
7	25	309	230	21.9	966	8.2	1.32	1.94
8	25	261	200	10.7	949	6.8	0.90	2.11
9	25	709	321	11.5	1350	18.4	1.17	2.17
10	25	470	176	11.6	1070	12.7	0.79	2.02
11	25	477	180	11.6	892	13.9	0.87	1.96
12	25	563	230	11.5	1400	16.6	0.91	2.05
13	25	569	239	11.8	1060	15.0	0.94	2.04
14	25	566	236	11.7	1320	15.8	0.95	2.16
15	25	566	237	11.7	1040	14.2	0.90	2.18
16	25	568	239	18.0	1230	14.6	0.91	2.26
17	12	736	236	15.4	1270	20.9	0.99	2.03
18	12	637	238	15.3	1290	19.6	0.80	1.94
19	12	1010	235	15.1	1280	23.9	0.73	2.11
20	12	557	236	15.4	1330	15.5	1.07	2.18
21	12	478	225	10.2	980	13.1	0.73	2.16
22	12	279	224	10.3	1000	9.2	1.20	2.21
23	12	369	227	10.4	1000	11.4	0.99	1.96

[a] The concentration of O_2 was 1.0×10^{17} molecules cm^{-3} in all experiments.

profile. We find that the most important interference is from ClO radicals, and as discussed above, ClO accounted for $\leq 5\%$ of BrO removal in all experiments. Two other side reactions occurring at short times are also worth mentioning. One such reaction is the Cl regeneration process

$$CH_2OH + Cl_2 \rightarrow Cl + CH_2ClOH \qquad (16)$$

Although CH_2OH is consumed via reaction 9 with a mean lifetime of 1 μs, up to 15% of generated CH_2OH can react with Cl_2 under the experimental conditions employed. Since reaction 16 regenerates Cl atoms, which in turn reinitiate the CH_2OH production chain, no net effect on the HO_2 yield results. A second rapid side reaction which operates to produce H atoms is of interest:

$$O(^1D) + CH_3OH \rightarrow H + CH_3O_2 \qquad (17)$$

Quenching by N_2/O_2 is the primary $O(^1D)$ loss process ($\tau = 40$ ns), but reaction 17 can convert up to 25% of $O(^1D)$ to H in the 12 Torr experiments. H atoms are subsequently taken up along three primary paths within 5 μs: (1) reaction with Cl_2 to produce Cl atoms and HCl, (2) reaction with Br_2 to produce Br atoms and HBr, and (3) reaction with O_3 to produce vibrationally excited OH. The Br and Cl atoms thus generated contribute to BrO and HO_2 production as shown in reactions 7−13. Vibrationally excited OH, which can be generated in up to 25% yield from H atoms, is deactivated rapidly by O_2 and CH_3OH, while ground-state OH is consumed within 50 μs by Br_2, CH_3OH, and HO_2 to produce Br, CH_2OH, and H_2O, respectively.

Results and Discussion

In the type of experiment reported in this paper, kinetic data must fulfill two criteria in order to be of value for quantitative determination of a rate coefficient for a radical−radical reaction. First, the temporal behavior of both reactants must be monitored with good signal-to-noise using techniques that allow absolute concentrations to be evaluated. Also, the reaction scheme must be such that the loss of the minor reagent (BrO in this study) is dominated by reaction with the excess reagent (HO_2 in this study). As discussed in some detail above, we believe that these two criteria are met in this study, albeit over a fairly narrow range of experimental conditions. The exact conditions used in all experimental runs used to obtain our reported value for k_1, i.e., all experimental runs that meet the above criteria, are given in Table 2. An unweighted average of the k_1 values obtained from individual experiments gives $k_1 = (2.04 \pm 0.24) \times 10^{-11}$ cm^3 molecule^{-1} s^{-1} where the uncertainty is 2σ and represents precision only.

The dominant source of uncertainty in our measurement of k_1 is not imprecision, but rather the uncertainty in the infrared line strength that has been used to evaluate the absolute concentration of HO_2. Zahniser et al. report the overall strength of the two coincident lines at 1371.927 cm^{-1} (which we have employed for HO_2 detection) to be $(1.2 \pm 0.3) \times 10^{-20}$ cm^2 molecule^{-1} cm^{-1} at 296 K.[16] Combining the uncertainty in the HO_2 concentration measurement with the uncertainties resulting from imprecision and our estimates of minor systematic errors from other sources, we report $k_1 = (2.0 \pm 0.6) \times 10^{-11}$ cm^3 molecule^{-1} s^{-1}. As mentioned above, the rate coefficient for the HO_2 self-reaction that we obtain using the infrared line strength of Zahniser et al. agrees very well with the recommended value,[14] which is based entirely on experiments where the HO_2 concentration was determined by chemical titration and/or by ultraviolet absorption measurements. This suggests that the Zahniser et al. line strength is actually quite accurate and that the reported error limits in our value for k_1 may be overly conservative.

Literature values for k_1 as well as for the activation energy of reaction 1 are summarized in Table 3. Reported values for k_1(298 K) fall into three groups: the slow rate coefficient reported many years ago by Cox and Sheppard,[3] the fast rate coefficients reported by the French groups from Orleans[4,6] and Bordeaux,[7] and the intermediate values reported recently by Elrod et al.,[8] Li et al.,[9] and in this study. The low-pressure discharge flow−mass spectrometry techniques employed by the Orleans[4,6] and JPL[9] groups are very similar although, as pointed out by Li et al.,[9] there are some differences in the HO_2 source

TABLE 3: Summary of Literature Values for the HO_2 + BrO Rate Coefficient

reference	technique[a]	P (Torr)	10^{11} k_1(298 K) (cm^3 $molecule^{-1}$ s^{-1})	E_a (kJ mol^{-1})
Cox and Sheppard (1980)[3]	MM/UV	760	0.5	
Poulet et al. (1992)[4]	DF/MS	1	3.3 ± 0.5	
Bridier et al. (1993)[7]	FP/UV	760	3.4 ± 1.0	
Larichev et al. (1995)[6]	DF/MS	1	3.3 ± 0.5	-4.82 ± 0.83
Elrod et al. (1996)[8]	DF/MS	100	1.4 ± 0.3	-4.32 ± 0.67
Li et al. (1997)[9]	DF/MS	1	1.73 ± 0.61[b]	-4.46 ± 1.71
			2.05 ± 0.64[c]	
this work	LFP/UV/TDLAS	25, 12	2.0 ± 0.6	

[a] MM/UV: molecular modulation/UV absorption. DF/MS: discharge-flow/mass spectrometry. FP/UV: flash photolysis/UV absorption. LFP/UV/TDLAS: laser flash photolysis/UV absorption/tunable diode laser absorption. [b] HO_2 was excess reagent. [c] BrO was excess reagent.

configurations. The only previous study that employed an experimental approach similar to ours is that of Bridier et al.,[7] who report the fast rate coefficient 3.4×10^{-11} cm^3 $molecule^{-1}$ s^{-1}. They used essentially the same photochemical scheme as we did; however, they generated radicals using a concentric flash lamp, monitored both HO_2 and BrO by UV absorption spectroscopy, and carried out experiments under conditions where the HO_2 and BrO concentrations were similar to one another in magnitude. Detection of HO_2 by UV absorption is subject to interferences from other radicals produced in side reactions (ClO, for example), while the use of non-pseudo-first-order conditions leads to increased uncertainty because observed temporal profiles are very sensitive to the absolute concentrations of both reactants.

Reaction 1 can proceed via multiple exothermic channels:

$$BrO + HO_2 \rightarrow HOBr + O_2 \quad (1a)$$

$$\rightarrow HBr + O_3 \quad (1b)$$

$$\xrightarrow{M} HO_2 \cdot BrO \quad (1c)$$

The apparent lack of a pressure dependence for k_1 (see Table 3) argues against the importance of channel 1c, and no positive evidence exists for the occurrence of this channel. While it is clear that reaction 1a is the dominant pathway for the HO_2 + BrO reaction, there is interest in establishing the branching ratio for channel 1b since this channel could represent an important source of stratospheric HBr even if k_{1b}/k_1 is quite small. Larichev et al.,[6] based on their inability to observe O_3 as a reaction product using mass spectrometric detection, have placed an upper limit of 0.015 on k_{1b}/k_1 over the temperature range 233−298 K. A much lower upper limit for k_{1b}/k_1 of $\sim 1 \times 10^{-4}$ has been suggested by Mellouki et al.[17] based on application of well-established thermochemistry in conjunction with measurement of a very low upper limit for the reverse reaction $HBr + O_3 \rightarrow HO_2 + BrO$; the implications of this very small value of k_{1b}/k_1 for our understanding of stratospheric bromine chemistry are discussed below.

Ab initio calculations of the structures and energetics of $HBrO_3$ isomers have recently been reported by Guha and Francisco;[18] they find the energy ordering to be $HOBrO_2$ < HOOOBr < HOOBrO < $HBrO_3$, with all isomers except $HBrO_3$ lying lower in energy than HO_2 + BrO. As pointed out by Li et al.,[9] it is unlikely that $HOBrO_2$ can form from HO_2 + BrO via a barrierless process as the observed negative activation energy for reaction 1 requires. Hence, reaction 1a probably proceeds via initial formation of HOOBrO and subsequent formation of a cyclic intermediate which decomposes to the products HOBr + O_2. While HOOBrO is apparently very weakly bound, Guha and Francisco predict that HOOOBr is 75 kJ mol^{-1} more stable than HO_2 + BrO. Given the very small observed value for k_{1b}/k_1 (see above), a significant barrier must exist toward conversion of HOOOBr to HBr + O_3 (via another cyclic intermediate). Hence even though (as mentioned above) no positive evidence exists for reaction 1c, a possible low-temperature channel producing HOOOBr warrants further investigation.

The results reported in this study support the slower values for k_1 reported by Elrod et al.[8] and Li et al.[9] and argue against the faster values reported by Poulet et al.,[4] Larichev et al.,[6] and Bridier et al.[7] The implications of employing the slower value for k_1 in models of stratospheric chemistry have been discussed by Li et al.[9] The overall rate of catalytic odd-oxygen destruction by bromine will be lowered a little and, as a result, the ozone depletion potential of CH_3Br will be slightly reduced. The slower value for k_1 will also result in repartitioning of some HOBr into BrO; hence, the reduction in the rate of the HO_2 + BrO catalytic cycle will be partially offset by an increase in the rates of other catalytic cycles involving BrO in the rate-limiting step (most notably the BrO + ClO cycle, i.e., reactions 3, 5, and 6).

Recent in situ balloon-based observations of HBr levels in the 20−36.5 km altitude range suggest an average daytime HBr mixing ratio of 1.31 ± 0.39 parts per trillion by volume;[19] at this level HBr is a non-negligible BrO_x reservoir. Reaction 1b has been considered a prime candidate in speculation concerning the source of stratospheric HBr. Model calculations by Lary[20] and Chartrand and McConnell[21] suggest that a branching ratio of about 0.01 for channel 1b would be required to account for observed levels of HBr. As discussed above, available laboratory data suggest that k_{1b}/k_1 is considerably less than 0.01.[17] One possible alternate source of stratospheric HBr could be a minor channel of the OH + BrO reaction, i.e., OH + BrO → HBr + O_2. On the basis of the only reported kinetics study of the OH + BrO reaction[22] and the model calculations of Chartrand and McConnell,[21] it appears that an HBr yield of around 0.03 would be required to account for observed levels of stratospheric HBr; an HCl yield of about 0.06 from the analogous OH + ClO reaction has recently been determined.[23]

Acknowledgment. This research has been supported through Grant NAG5-3634 from the National Aeronautics and Space Administration—Upper Atmosphere Research Program.

References and Notes

(1) Wofsy, S. C.; McElroy, M. B.; Yung, Y. L. *Geophys. Res. Lett.* **1975**, *2*, 215.

(2) Yung, Y. L.; Pinto, J. P.; Watson, R. T.; Sander, S. P. *J. Atmos. Sci.* **1980**, *37*, 339.

(3) Cox, R. A.; Sheppard, D. W. *J. Chem. Soc., Faraday Trans. 2* **1982**, *78*, 1383.

(4) Poulet, G.; Pirre, M.; Maguin, F.; Ramoroson, R.; Le Bras, G. *Geophys. Res. Lett.* **1992**, *19*, 2305.

(5) Wennberg, P. O.; Cohen, R. C.; Stimpfle, R. M.; Koplow, J. P.; Anderson, J. G.; Salawitch, R. J.; Fahey, D. W.; Woodbridge, E. L.; Keim, E. R.; Gao, R. S.; Webster, C. R.; May, R. D.; Toohey, D. W.; Avallone, L. M.; Proffitt, M. H.; Loewenstein, M.; Podolske, J. R.; Chan, K. R.; Wofsy, S. C. *Science* **1994**, *266*, 398.

(6) Larichev, M.; Maguin, F.; Le Bras, G.; Poulet, G. *J. Phys. Chem.* **1995**, *99*, 15911.

(7) Bridier, I.; Veyret, B.; Lesclaux, R. *Chem. Phys. Lett.* **1993**, *201*, 563.

(8) Elrod, M. J.; Meads, R. F.; Lipson, J. B.; Seeley, J. V.; Molina, M. J. *J. Phys. Chem.* **1996**, *100*, 5808.

(9) Li, Z.; Friedl, R. R.; Sander, S. P. *J. Chem. Soc., Faraday Trans.* **1997**, *93*, 2683.

(10) Ravishankara, A. R.; Wine, P. H.; Nicovich, J. M. *J. Chem. Phys.* **1983**, *78*, 6629.

(11) Nicovich, J. M.; Wine, P. H. *J. Phys. Chem.* **1987**, *91*, 5118.

(12) Nicovich, J. M.; Wine, P. H.; Ravishankara, A. R. *J. Chem. Phys.* **1988**, *89*, 5670.

(13) Thorn, R. P.; Cronkhite, J. M.; Nicovich, J. M.; Wine, P. H. *J. Chem. Phys.* **1995**, *102*, 4131.

(14) DeMore, W. B.; Sander, S. P.; Golden, D. M.; Hampson, R. F.; Kurylo, M. J.; Howard, C. J.; Ravishankara, A. R.; Kolb, C. E.; Molina, M. J. *Chemical Kinetics and Photochemical Data for Use in Stratospheric Modeling*; Evaluation No. 12, Jet Propulsion Laboratory Pulbication No. 97−4, 1997.

(15) Wahner, A.; Ravishankara, A. R.; Sander, S. P.; Friedl, R. R. *Chem. Phys. Lett.* **1988**, *152*, 507.

(16) Zahniser, M. S.; McCurdy, K. E.; Stanton, A. C. *J. Phys. Chem.* **1989**, *93*, 1065.

(17) Mellouki, A.; Talukdar, R. K.; Howard, C. J. *J. Geophys. Res.* **1994**, *99*, 22949.

(18) Guha, S.; Francisco, J. S. *J. Phys. Chem. A* **1998**, *102*, 2072.

(19) Nolt, I. G.; Ade, P. A. R.; Alboni, F.; Carli, B.; Carlotti, M.; Cortesi, U.; Epifani, M.; Griffin, M. J.; Hamilton, P. A.; Lee, C.; Lepri, G.; Mencaraglie, F.; Murray, A. G.; Park, J. H.; Park, K.; Raspollini, P.; Ridolfi, M.; Vanek, M. D. *Geophys. Res. Lett.* **1997**, *24*, 281.

(20) Lary, D. J. *J. Geophys. Res.* **1996**, *101*, 1505.

(21) Chartrand, D. J.; McConnell, J. C. *Geophys. Res. Lett.* **1998**, *25*, 55.

(22) Bogan, D. J.; Thorn, R. P.; Nesbitt, F. L.; Stief, L. J. *J. Phys. Chem.* **1996**, *100*, 14383.

(23) Molina, M. J. Private communication.

(24) Nicovich, J. M.; Wine, P. H. *Int. J. Chem. Kinet.* **1990**, *22*, 379.